Energy Advances

ROYAL SOCIETY OF CHEMISTRY

PAPER

View Article Online
View Journal

Cite this: DOI: 10.1039/d5ya00172b

Competing ion effects and electrolyte optimization for electrochemical lithium extraction from spent lithium iron phosphate battery cathodes

Stefanie Arnold [ab] and Volker Presser *[abc]

With rising demand for lithium-ion batteries, efficient recycling is crucial. While conventional methods face cost and environmental challenges, electrochemical recovery offers a sustainable and energy-efficient alternative. In this study, we investigate the electrochemical recovery of lithium-ions from spent lithium iron phosphate batteries using carbon-coated lithium iron phosphate electrodes, with a focus on the influence of pH adjustment and competing ion effects. Our results demonstrate that NaOH-adjusted electrolytes provide the highest lithium-ion recovery efficiency, with an average removal capacity of 18 mg_{Li} g_{LFP}^{-1} over 50 cycles. However, prolonged cycling leads to capacity fading, particularly in the presence of competing cations such as Na^+ and K^+, which impact lithium selectivity and electrode stability. These findings underscore the importance of optimizing electrolyte conditions and electrode materials to enhance long-term performance. Future research should explore alternative pH control strategies and scalable process designs to facilitate industrial implementation. Advancing electrochemical lithium-ion recovery aligns with broader sustainability goals, offering a viable route toward circular battery recycling and reduced environmental impact.

Received 26th June 2025,
Accepted 1st August 2025

DOI: 10.1039/d5ya00172b

rsc.li/energy-advances

1. Introduction

Lithium-ion batteries now play a pivotal role in powering electric vehicles and portable electronics, driving a surge in global demand for lithium.[1,2] As electrification accelerates, the extraction of lithium reserves is likely to cause substantial price increases for the metal.[3] Furthermore, securing these resources presents challenges, including geopolitical tensions, ethical concerns over labor practices, and environmental damage associated with mining operations, particularly in politically volatile regions.[4] Beyond finite supply constraints, ecological impact and long-term sustainability have become critical factors in evaluating lithium extraction.[5] In response, the European Commission has introduced stricter regulations to promote greener, safer, and more circular battery production. These rules include phased recycling targets for battery materials, with mandatory minimum recovery rates set to take effect starting in 2024.[6]

Typical batteries for electric devices usually consist of a variety of raw materials. The anode is usually composed of a mixture of graphite with conductive carbon black and a polymeric binder, which will be applied to a current collector. In a similar process, the cathode electrode is manufactured. A significant portion of the costs falls on the cathode material, which typically consists of lithium and other battery metals, such as cobalt, nickel, and manganese, and determines the battery's capacity and power.[7,8] Recent advancements in battery technology have introduced multiple cathode materials, including nickel–manganese–cobalt oxide (NMC), lithium cobalt oxide (LCO), alumina-doped nickel–cobalt oxide (NCA), lithium manganese oxide (LMO), and lithium iron phosphate ($LiFePO_4$), all of which have contributed significantly to the evolution of modern batteries.[9–11] These various cathode materials also contribute differently in terms of cost and mass share in the overall battery, primarily because they contain a significant amount of critical and scarce metals, such as lithium, cobalt, nickel, and manganese.

As lithium has emerged as both a critical raw material and strategic element for electromobility, there is an urgent need to investigate and evaluate novel recycling approaches from an economic perspective, particularly for the expanding battery sector. Current state-of-the-art recycling methodologies for end-of-life batteries have predominantly utilized hydrometallurgical

[a] INM - Leibniz Institute for New Materials, Campus D2 2, 66123, Saarbrücken, Germany. E-mail: volker.presser@leibniz-inm.de
[b] Department of Materials Science and Engineering, Saarland University, Campus D2 2, 66123, Saarbrücken, Germany
[c] saarene - Saarland Center for Energy Materials and Sustainability, Campus D4 2, 66123, Saarbrücken, Germany

and pyrometallurgical processes, targeting the recovery of valuable metals including cobalt, copper, nickel, manganese, zinc, and iron.[12] Pyrometallurgical recycling has emerged as a preeminent and well-established method, owing to its concise reaction duration, elevated efficiency, and scalability. The principal pyrometallurgical techniques employed for recycling spent lithium-ion batteries include pyrolysis, incineration, roasting, and smelting. The fact that most traditional industrial pyrometallurgical processes are not optimized for lithium-ion recovery, combined with the high energy requirements and the complex off-gas treatment, leads to a need to develop a resource-efficient recycling method.[13–15]

Hydrometallurgy recycling processes need the insertion of high amounts of chemicals like hydrochloric acid (HCl), nitric acid (HNO_3), sulfuric acid (H_2SO_4), citric acid ($C_6H_8O_7$), phosphoric acid (H_3PO_4), ascorbic acid ($C_6H_8O_6$), or oxalates ($H_2C_2O_2$).[16–18] As a result, byproducts are often generated, and gases such as Cl_2 or NO_x are released.[19,20] At the same time, industrial processes are primarily designed for the recovery of nickel, cobalt, and manganese.[21] However, due to the rapid advancements in battery technology and the continuous evolution of individual battery components, there is a growing need for cost-effective and flexible recycling methods that can be adapted for industrial applications.[8,22]

The projected sustained increase in lithium costs, coupled with evolving policy-driven regulatory frameworks, is poised to intensify industry-wide adoption and scaling of lithium recycling initiatives. Among emerging technologies, ion-selective electrochemistry presents particularly promising potential, offering both economic viability and environmental benefits. This advanced approach enhances conventional hydrometallurgical methods while facilitating effective lithium-ion recovery.[23]

The first approaches propose electrochemical processes for recycling cobalt and nickel through galvanostatic electrowinning and potentiostatic electrolysis.[24] Thereby, a good cobalt and nickel deposit was achieved, showing current efficiencies of 96% and 87%, and specific energy consumption of 2.8 kWh kg^{-1} and 3.0 kWh kg^{-1}, respectively.[24] Further, Asl *et al.* demonstrate the electrochemical collection of lithium metal from a waste lithium-ion battery.[25] This study also illustrated that the lithium metal obtained from discarded lithium-ion batteries could serve as the anode within the battery system, resulting in a voltage of 2.7 V at a current density of 0.1 mA cm^{-2} when water was employed as the cathode.[25] Electrochemical recycling can be very versatile, starting from electrode material recycling and recycling ions out of a liquid solution. Ribeiro *et al.* have reported a study detailing the synthesis of a hybrid material derived from recycled lithium-ion batteries through a hydrometallurgical process.[26] After reprocessing, this material combines reduced graphene oxide with cobalt oxide and exhibits impressive capabilities as an enzyme-free electrochemical sensor.[26] Further, Nie *et al.* introduced the possibility of recycling the spent $LiMn_2O_4$ cathode of a spent lithium-ion battery to be used directly as a cathode in sodium-ion batteries.[27] With this approach, the $LiMn_2O_4$ shows high sodium-storage properties with a capacity of 163 mAh g^{-1} over 50 cycles at 100 mA g^{-1}.[27]

Li *et al.* published a work in which free-standing MXene ($Ti_3C_2T_z$) electrodes, free of binder and conductive additives, were applied as electrodes in lithium-ion and sodium-ion batteries.[28] After reaching the end of their life, the electrodes underwent a direct recycling process, resulting in capacity retention for both systems of higher than 90%. If not suitable for direct re-use, it is also possible to oxidize the MXene into TiO_2/C materials. These materials hold significant promise for secondary use in the battery industry and beyond, particularly in applications related to electrochemical oxygen conversion, photocatalytic hydrogen production, or photodegradation.[28] In 2012, Pasta *et al.* introduced an innovative electrochemical approach for lithium extraction from brines, utilizing desalination battery technology to achieve energy-efficient recovery.[29] The device was equipped with a lithium-ion-selective $LiFePO_4$ electrode and a chloride-capturing silver (Ag) electrode. It adeptly facilitated the conversion of a sodium-rich brine (characterized by a lithium-to-sodium ratio of 1 : 100) into a lithium-ion-rich solution (featuring a lithium-to-sodium ratio of 5 : 1) while exhibiting an energy consumption rate of merely 144 Wh per kilogram of lithium.[29] A study of Nam *et al.* in 2025 introduced an innovative electrochemical system, comprising a lithium ion extraction cell and a lithium ion recovery cell, that efficiently recycles lithium from spent $LiFePO_4$ batteries as Li_3PO_4, Li_2CO_3, or LiOH through simple, low-cost processes.[30] The system regenerates the acid used for Li^+ leaching, thereby reducing chemical consumption and waste generation, and enabling an environmentally sustainable recycling approach.[30]

In this work, we investigate an electrochemical method for recovering lithium-ions from spent LFP batteries using carbon-coated LFP electrodes, with a focus on pH optimization and the effects of competing ions. In our lithium-ion recovery application from spent lithium iron phosphate batteries, we employed a electrochemical technique following a wet chemical digestion of the battery material. Therefore, we implemented a lithium-ion-selective lithium iron phosphate in combination with a permselective carbon counter electrode. Based on this, an average removal capacity of 18 mg Li per gram of $LiFePO_4$ electrode was obtained for 50 cycles when adjusting the pH of the leaching solution with NaOH. Adjusting with other bases like KOH, $Ca(OH)_2$, and NH_4OH leads to poorer performance or lower selectivity.

2. Experimental

2.1. Materials synthesis

2.2.1. Synthesis of $LiFePO_4$ nanoplates. The synthesis of $LiFePO_4$ nanoplates was performed by optimizing a synthesis route given in the literature.[31] In detail, the synthesis consists of two steps, starting with a neutralization reaction of H_3PO_4 with LiOH to obtain anhydrous Li_3PO_4. Therefore, a lithium hydroxide solution containing 0.5 M Li^+ was prepared by dissolving 4.22 g of $LiOH{\cdot}H_2O$ in 350 mL of deionized water.

Sequentially, 3.72 mL of H_3PO_4 (65 mass%) was gradually introduced into the solution over 5 min under magnetic stirring, resulting in the formation of a white suspension. Following an additional 15 min of magnetic stirring at room temperature, the resultant suspension underwent filtration using a porous polyvinylidene difluoride (PVdF) membrane filter with a pore size of 0.22 μm. The product was rinsed with water multiple times before being dried at 110 °C for 12 h. The $FeSO_4{\cdot}H_2O$ powders were obtained by heat treatment at 100 °C for 12 h under vacuum conditions of the commercial $FeSO_4{\cdot}7H_2O$.

For the $LiFePO_4$ synthesis, 27.2 g Li_3PO_4 (234.8 mmol) was dissolved in 120 mL ethylene glycol under stirring in a 200 mL polytetrafluoroethylene autoclave. Subsequently, 8 mL H_3PO_4 (85 mass%) was added slowly to the reaction solution. After thorough mixing, $FeSO_4{\cdot}H_2O$ (39.9 g, 234.8 mmol) and ascorbic acid (0.8 g, 4 mmol) are added to the reaction mixture to give a ratio of Li : Fe : P = 3 : 1 : 1.5. The autoclave was heated to 180 °C for 2.5 h. After cooling, the product was filtered and washed with deionized water (less than 0.056 μS cm^{-1} at 25 °C, Milli-Q). The resulting green powder was dried at 60 °C for 12 h.

2.1.2. Carbon coating of $LiFePO_4$. Carbon coating of the $LiFePO_4$ particles was conducted using a two-step method similar to previous works.[32,33] 0.36 g of citric acid was dissolved in 20 mL of Milli-Q water and transferred to a small beaker, and stirred for 2 min until a clear solution formed. Then, 0.36 mL of ethylene glycol (0.42 g) was added to the solution. Finally, 0.8 g $LiFePO_4$ was added to the solution, and the reaction mixture was heated to 80 °C in an oil bath (stirring speed was 200 rpm). After 90 min, heating was stopped, and a slurry-like suspension was formed, indicating that the alkyl ester surrounds the $LiFePO_4$ particles. Subsequently, the alkyl ester coated $LiFePO_4$ underwent a carbonization process within an argon environment, involving a two-stage heating procedure. Initially, the IR furnace temperature was set to +200 °C for a duration of 2 h, facilitating the elimination of moisture content from the materials. This was followed by heating the specimen to 700 °C and maintaining this temperature for 6 h, resulting in the formation of the hybrid $LiFePO_4$/carbon composite material.

2.2. Material characterization

Scanning electron microscopy (SEM) was performed using a Carl Zeiss Gemini 500 scanning electron microscope operated at 1 kV accelerating voltage. Specimens were mounted on aluminum stubs with double-sided copper conductive tape and analyzed without sputter coating.

X-ray diffraction analysis was conducted on a Bruker AXS D8 Discover system configured with a copper X-ray source (Cu Kα, λ = 1.5406 Å) operating at 40 kV and 40 mA, featuring a Göbel mirror and 1 mm point focus. Using a VANTEC-500 area detector positioned at three distinct 2θ angles (17°, 37°, 57°), four frames were acquired with 1000 s exposures per position. The powder samples were fixed on a glass sample holder with a depth of 0.5 mm. All scans went through background subtraction and were normalized to (0–1).

Raman spectroscopy was performed using a Renishaw inVia microscope system with a 532 nm Nd-YAG laser (0.05 mW power output). Measurements employed a 50× objective (aperture of 0.75) and 2400 mm grating, collecting data from five sample locations (5 accumulations, 30 s exposure each). The powder samples were mounted on glass microscope slides. A normalization procedure was applied, standardizing all spectra to a range between 0 and 1. Automated cosmic ray removal was employed on the acquired spectra. A silicon standard was utilized to calibrate the system before and after the measurements.

Inductively coupled plasma optical emission spectrometry analyses were conducted using a Horiba Jobin Yvon Ultima 2 system, examining both pristine and cycled samples. The instrument configuration included a conical nebulizer operating at 271 kPa pressure with a 0.9 L min^{-1} flow rate. Elemental concentrations were determined at characteristic emission lines: aluminum 396.152 nm; Cu 327.395 nm; Fe 238.207 nm; Li 670.791 nm; Na 589.592 nm.

2.3. Leaching solution preparation

The leaching solution of spent $LiFePO_4$ batteries was obtained by chemical digestion (Fig. 3B). The spent batteries used in this study were commercial RS Pro $LiFePO_4$ 18650 cylindrical cells (RS Components GmbH, nominal voltage: 3.2 V, capacity: 1600 mAh). Prior to disassembly, the cells were fully discharged to 0 V to ensure safety. The outer casing was mechanically removed, and the cathode ($LiFePO_4$-coated Al foil), anode (graphite-coated Cu foil), and separator were separated manually. The cathode electrode coatings (including aluminum current collectors) underwent thermal treatment at 800 °C for 12 h in atmospheric air using a muffle furnace (IFR GmbH) to pyrolyze polymeric binders, organic components, or residual electrolytes. For acid leaching, 1.6 g of the calcined product was reacted with 80 mL of 4 M hydrochloric acid in a reflux system maintained at 80 °C for 1 h. The cooled yellow solution was then isolated by vacuum filtration. A small residue with insoluble components remained. Concentrations of specific present ions were analyzed *via* ICP-OES.

To apply the obtained leaching solution as an electrolyte for lithium recycling, the pH of the solution was adjusted to 5–6 with different powder bases ($Ca(OH)_2$, NH_4OH, KOH, NaOH, $Al(OH)_3$) (Sigma Aldrich). While vigorously stirring the leaching solution and cooling it in an ice bath, the solution (NH_4OH) or flakes of the bases were added dropwise or portion-wise, and the pH value development was monitored using a pH module (Metrohm, 867 pH module) controlled by the Tiamo software.

2.4. Electrode materials and electrode preparation

$LiFePO_4$/carbon-coated $LiFePO_4$ electrodes were prepared with a composition of 80 mass% $LiFePO_4$/carbon-coated $LiFePO_4$, 10 mass% acetylene black (Alfa Aesar, 99.5%), and 10 mass% PVdF (Sigma Aldrich) dissolved in *N*-methyl-2-pyrrolidone (NMP) following the mixing steps described below.

Initial mixing of $LiFePO_4$/carbon-coated $LiFePO_4$ with conductive carbon was performed through dry grinding in a

mortar. The powder mixture was subsequently processed in a Hauschild SpeedMixer DAC 150 SP at 1000 rpm for 5 min. NMP was then introduced dropwise to adjust slurry viscosity, followed by sequential mixing at 1500 rpm (5 min) and 2500 rpm (5 min). Finally, the PVdF binder solution (10 mass% PVdF in NMP) was added, and the viscous electrode paste was mixed at 800 rpm for 10 min.

The slurry was magnetically stirred for 12 h to ensure homogeneity before doctor-blade coating onto graphite paper (SGL, 300 μm substrate) with 200 μm wet thickness. After ambient drying overnight, electrodes were vacuum-dried at 100 °C for 12 h to eliminate residual solvent. Afterward, discs of 12 mm diameter were punched from the coating using a press-punch (EL-CELL) and applied as the working electrode (WE). The resulting electrode thickness of the dried electrodes was 65–65 μm with a material loading of 2.7 mg cm^{-2}.

2.5. Cell preparation and electrochemical characterization

Custom cells made from polyether ether ketone (PEEK) with spring-loaded titanium pistons were employed to conduct electrochemical half-cell tests.[34] These cells were configured in sets of three electrodes to facilitate electrochemical measurements. The electrode disks were punched from the electrode films and had a diameter of 12 mm (equivalent to 1.13 cm^2). An Ag/AgCl (3 M NaCl $E_{0\,Ag/AgCl}$ = 0.210 V *vs.* normal hydrogen electrode, BASi) electrode served as a reference electrode. The assembly process began with placing the 12 mm diameter $LiFePO_4$/carbon-coated $LiFePO_4$ working electrode within the cell, followed by a vacuum-dried, 13 mm diameter compressed glass-fiber separator (GF/A, Whatman). The oversized counter electrode, consisting of Kynol ACC-507-20, was shaped as circular plates with a diameter of 10 mm and placed on top of the separator. A graphite paper current collector was attached to the backside of each counter electrode. Near the working electrode and counter electrode stack, the reference electrode was situated on a compressed glass-fiber separator (GF/A, Whatman) with a diameter of 3 mm. The remaining three holes were sealed using PEEK screws. The cell was filled with 35 mM LiCl/battery leaching solution electrolyte by vacuum backfilling using a syringe.

All electrochemical tests were performed using a VMP3 multi-channel potentiostat/galvanostat from Bio-Logic, which included galvanostatic cycling with potential limitation (GCPL) and cyclic voltammetry (CV). All these measurements were carried out in a climate chamber (Binder) maintained at a constant temperature of +25 ± 1 °C, ensuring consistent conditions. During the galvanostatic charge/discharge cycling with potential limitation (GCPL) experiments, voltage recordings were made within the range of −0.3 V to +0.4 V *vs.* Ag/AgCl. We used a specific current of 50 mA g^{-1} throughout measurements. Additionally, all cyclic voltammetry measurements were carried out using a scan rate of 1 mV s^{-1}, encompassing a potential window spanning from −0.3 V to +0.4 V *vs.* Ag/AgCl. The controlled environment and carefully chosen parameters allowed for accurate and reliable analysis of the electrochemical characteristics.

2.6. Electrochemical desalination and ion selectivity

For selectivity tests, a custom-built multi-channel cell was employed. This cell consists of two side channels made of acrylic glass and one middle channel through which the aqueous electrolyte can flow. The cell's airtight seal is ensured by using diverse silicon gaskets with a thickness of 600 μm. The electrodes (coated on graphite paper) were resting on graphite blocks measuring 5 × 5 cm^2 with a thickness of 10 mm. The working electrode consists of a 30 mm diameter carbon-coated $LiFePO_4$ electrode. The counter electrode consists of three pieces of 30 mm diameter carbon cloth (Kynol 5092-10) discs, which are in direct contact with a graphite current collector. The anode and cathode are separated with a water flow channel filled with nylon mesh to prevent the electrodes from collapsing, prevent the cell from short-circuiting, and maintain electrical contact between the two sides. Directly on top of the Kynol electrode, three glass fiber separators (GF/A, Whatman) were placed before a nonreinforced 31 ± 2 μm anion-exchange membrane (Fumatech, FAS-30) with a diameter of 50 mm was added. Before the experiment, the electrodes were charged with a current of 0.1 A g^{-1}, with a potential limitation of 0.4 V *vs.* Ag/AgCl, in a three-electrode system using aqueous 1 M LiCl, to remove reversibly stored cations already present in the electrode beforehand. During operation, the electrochemical cell undergoes cycles of discharge and charging, utilizing the battery-leaching solution as its electrolyte. The electrolyte is consistently circulated through the cell from a stationary reservoir with a flow rate of 5 mL min^{-1}. We discharged the cell only into the leaching solution to absorb lithium at the working electrode and analyze the uptake capacity over specific cycles. In the next step, the cell was flushed with ultra-pure water for 30 min to remove ions that were not stored. Afterward, we charged the cell in the recovery solution consisting of 15 mL of a 10 mM NaCl solution. The uptake capacity is determined *via* the following equations:

$$\text{Lithium ion uptake capacity } \left(\text{mg g}^{-1}\right) = \frac{V \times (c - c_{\text{initial}})}{m_{\text{electrode}}} \quad (1)$$

where V is the volume of the reservoir (in L), c_{initial} and c the concentration of Li^+ before and after treatment (in mg L^{-1}), and $m_{\text{electrode}}$ characterizes the mass of the electrode (in g).

$$K_{\text{Li/M}} = \frac{\Delta c_{\text{Li}}}{\Delta c_{\text{M}}} \times \frac{c_{\text{M-initial}}}{c_{\text{Li-initial}}} \quad (2)$$

whereby Δc_{Li} and Δc_{M} demonstrate the concentration change of Li^+ or M (M = Ca^{2+}) (in mmol); $c_{\text{Li-initial}}$ and $c_{\text{M-initial}}$ are the initial concentrations of Li^+ or M (in mmol L^{-1}).

3. Results and discussion

3.1. $LiFePO_4$ synthesis and material characterization

One way for selective extraction of lithium ions from aqueous solutions is to investigate electrode materials that have been extensively researched in the context of lithium-ion batteries and possess sufficient stability in aqueous environments. A prominent example is lithium iron phosphate ($LiFePO_4$), which is already commercially employed in batteries, readily available

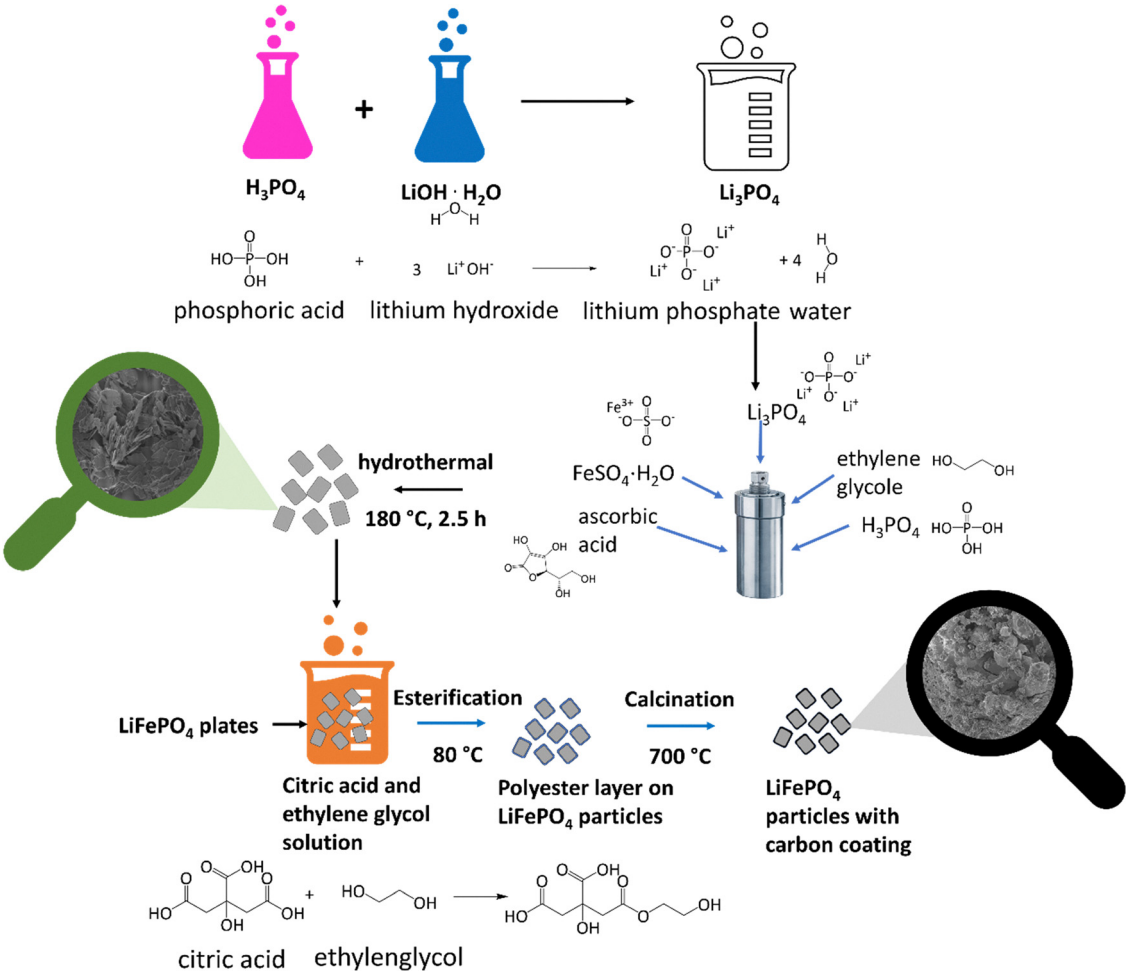

Fig. 1 Schematic representation of the reaction mechanism and synthesis parameters of the $LiFePO_4$ particles and the respective carbon coating.

in large quantities, and has also been the subject of recycling initiatives.[35–38] In this work, therefore, we employed a one-pot, template-free synthesis route to obtain [100]-oriented $LiFePO_4$ nanoflakes.[31] The main procedure of the synthesis is displayed in Fig. 1. After the acid–base reaction to obtain pure and water-free lithium phosphate, $LiFePO_4$ nanoflakes were synthesized *via* a one-pot solvothermal method at 180 °C for 2.5 h. The obtained green-gray powder was characterized *via* XRD, and the corresponding X-ray diffractogram is shown in Fig. 2A. The well-defined reflections can be clearly assigned to orthorhombic $LiFePO_4$ with the space group of *Pnma* (space group number 62; PDF card number 01-081-1173).

The morphology of the $LiFePO_4$ comprised a flake-like appearance with a particle length and width of around 200 nm, while the thickness is about 20 nm (Fig. 2C). Our past work established that the introduction of a carbon layer on the surface of $LiFePO_4$ particles improves performance stability in aqueous media while delivering additional conductivity.[32] In a further step, the synthesized flake-shaped $LiFePO_4$ particles are covered with a carbon layer. This was done by esterifying citric acid and ethylene glycol, which form a polyester compound around the $LiFePO_4$. In a subsequent heating step, this coating was transferred to a graphitized carbon layer.[33]

The X-ray diffractogram for $LiFePO_4$@C (Fig. 2B) remains in good agreement with the orthorhombic $LiFePO_4$, indicating that the carbon-coating process does not affect the inherent structure of $LiFePO_4$. However, a slight increase in baseline noise suggests the presence of the amorphous carbon layer. The morphology after carbon coating (Fig. 2C) changed significantly from the flake-like structure observed for pristine $LiFePO_4$ (Fig. 2C) to more agglomerated and rounded particles, likely due to the polymer-based coating process and subsequent heat treatment.

The presence of the carbon coating was further verified by Raman spectroscopy (Fig. 2D), where the coated $LiFePO_4$ sample exhibits two distinct peaks at approximately 1350 cm^{-1} (D-band) and 1580 cm^{-1} (G-band), corresponding to disordered and graphitic carbon, respectively. In contrast, the uncoated $LiFePO_4$ (Fig. 2D) lacks these characteristic carbon-related features, confirming the absence of sp^2-hybridized carbon structures in the pristine material. The Raman spectrum of the synthesized $LiFePO_4$ (Fig. 2D) exhibits characteristic vibrational modes associated with the phosphate (PO_4^{3-}) group and Fe–O interactions within the orthorhombic olivine structure. The most prominent peaks are typically observed in the range of 900–1000 cm^{-1}, which corresponds to the symmetric and

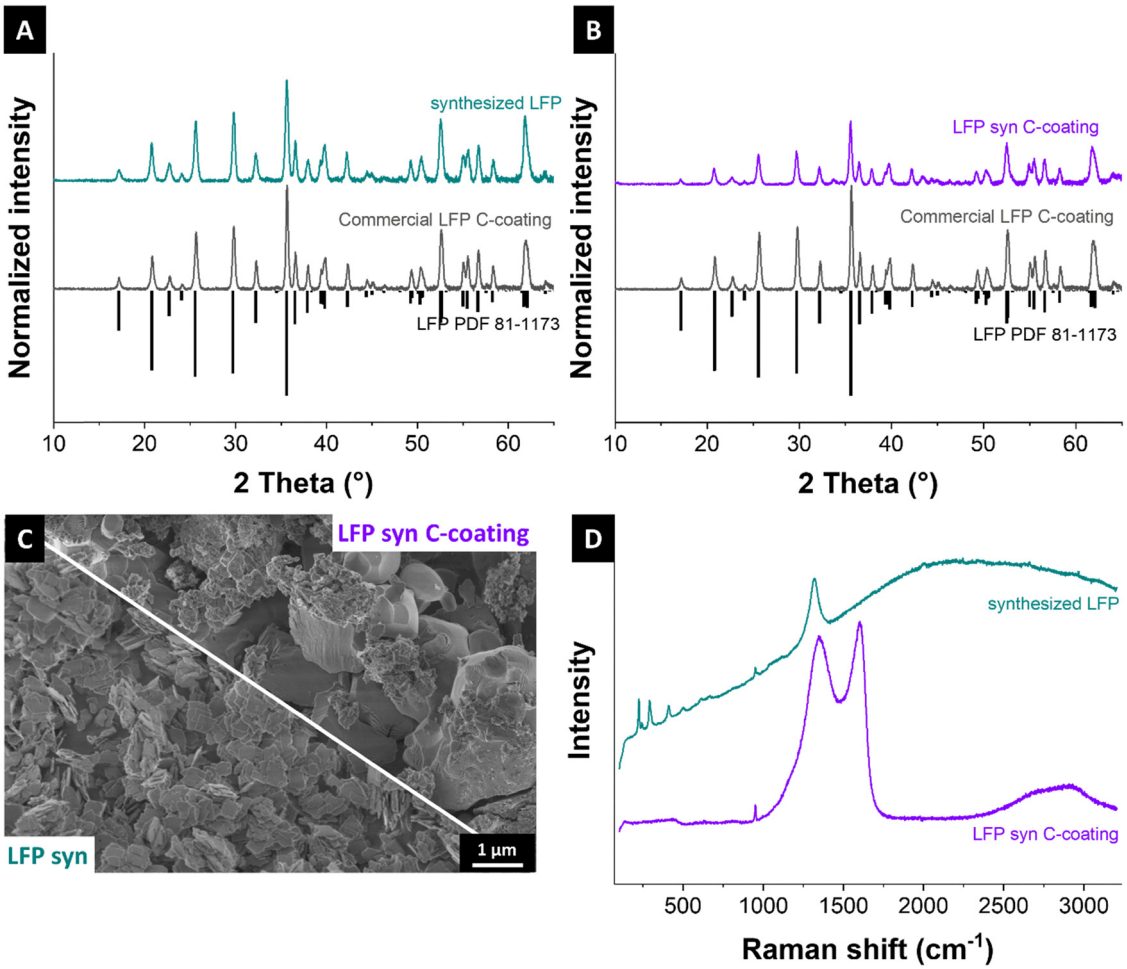

Fig. 2 Chemical characterization of the as-synthesized and carbon-coated $LiFePO_4$. (A) X-ray diffractograms using Cu-Kα radiation for the synthesized $LiFePO_4$ in comparison to commercial $LiFePO_4$. (B) X-ray diffractograms for carbon-coated synthesized $LiFePO_4$ in comparison to commercial carbon-coated $LiFePO_4$. (C) Scanning electron micrograph of as-synthesized $LiFePO_4$ and carbon-coated $LiFePO_4$. (D) Raman spectra of as-synthesized $LiFePO_4$ and carbon-coated $LiFePO_4$.

asymmetric stretching vibrations of the P–O bonds in the PO_4^{3-} tetrahedra.[39] The weaker signals below 600 cm^{-1} are attributed to Fe–O vibrations, which are associated with the movement of Fe^{2+} ions within the $LiFePO_4$ lattice. The relatively broad features in the spectrum might indicate a degree of structural disorder or the presence of minor secondary phases. However, the overall spectral shape is consistent with well-crystallized $LiFePO_4$. These findings indicate the successful formation of a conductive carbon coating, which is expected to enhance the electrochemical performance of $LiFePO_4$. As demonstrated in our prior work, carbon coating on $LiFePO_4$ will just add about 3 mass% of additional carbon to the material.[40] This engineered carbon layer enhances electronic conductivity and electrode/electrode–electrolyte interface stability while maintaining full electrochemical activity by minimizing inactive mass.

3.2. Leaching solution

Our developed lithium chloride extraction method from spent LIB cathodes comprises four key steps: (1) high-temperature calcination, (2) acid leaching of metal salts, (3) solution pH optimization, and (4) electrochemical lithium recovery. For electrochemical lithium-ion recovery, the ions need to be present in the form of a liquid solution. Therefore, the extracted cathode electrode, after a calcination step to remove organic compounds as a binder, underwent a leaching process. We employed HCl as an inorganic acid to serve as the leaching reagent because of its low price and high leaching efficiency.[41,42]

Wang *et al.* determined that employing a 4 M hydrochloric acid solution, maintaining an 80 °C leaching temperature, conducting leaching for 1 h, and using a solid-to-liquid ratio of 0.02 g mL^{-1} could yield a leaching efficiency exceeding 99% for Co, Mn, Ni, and Li.[41] We followed this approach, which resulted in a dark yellow solution with a few leftover red or orange particles that could not be dissolved. Since our electrochemical approach utilizes a selective electrode material that cannot operate in drastic pH conditions (such as 0 for the 4 M HCl solution), a pH adjustment step was implemented.[40] The choice of different reagents for this purpose will have a direct effect on the recovery process due to the different behaviors of

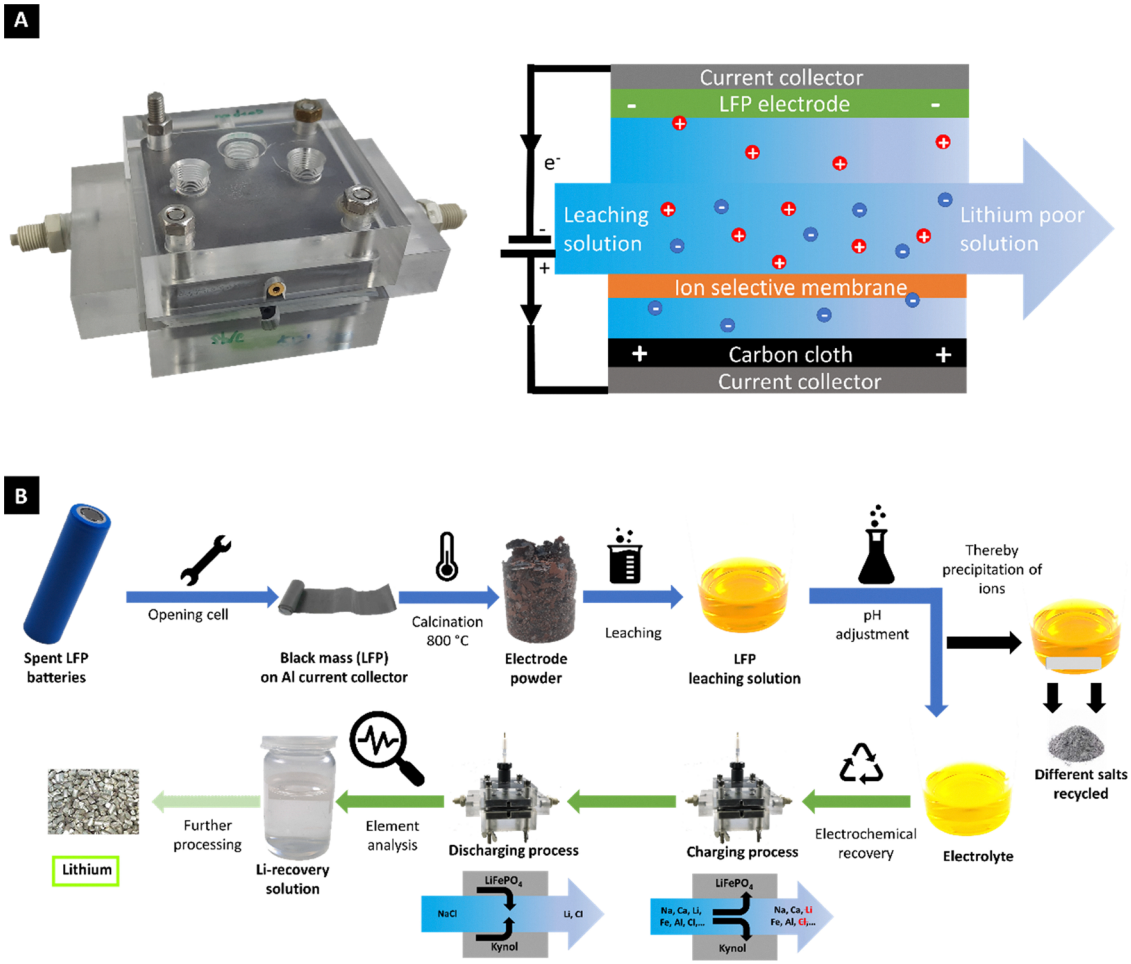

Fig. 3 (A) Photograph and (B) schematic drawing of the lithium-ion recovery cell used for this work. (C) Schematic drawing of the process steps done for the lithium recycling from spent LIB batteries.

different competing ions. Starting from a divalent and cheap component, we adjusted the pH of the leaching solution first with $Ca(OH)_2$ and evaluated the electrochemical behavior. In further steps, pH adjustment was conducted with NH_4OH, KOH, NaOH, and $Al(OH)_3$ (Fig. 3B). The concentrations of all ions before and after pH adjustment are presented in Table 1.

3.3. Electrochemical characterization

3.3.1. Electrochemical characterization of the $LiFePO_4$. Before initiating the recovery process, an evaluation was conducted on the synthesized material using an artificial leaching solution mirroring the lithium concentration of the original solution (35 mM LiCl, Table 1). This evaluation employed cyclic voltammetry to characterize the redox behavior of the electrode material. Fig. 4A and B display the first three cyclic voltammograms of the as-synthesized $LiFePO_4$ and the carbon-coated $LiFePO_4$. Both cyclic voltammograms share similar shapes, exhibiting the characteristic redox peaks. Reduction occurs around 0.05 V *vs.* Ag/AgCl, while oxidation takes place at approximately 0.2 V *vs.* Ag/AgCl. The carbon-coated $LiFePO_4$ material showcases higher redox peak currents, indicating its superior suitability as an electrode material for lithium-ion recovery.

The relevant cycling stability of both $LiFePO_4$ electrodes was tested for 300 cycles at a specific current of 50 mA h g^{-1} in a potential range between −0.3 V and +0.6 V *vs.* Ag/AgCl. The corresponding galvanostatic charge and discharge curves are displayed in Fig. 4C and D, highlighting distinct differences between the two electrodes. While the carbon-coated $LiFePO_4$ demonstrates plateaus corresponding to the redox reactions, as observed in cyclic voltammogram measurements, the as-synthesized $LiFePO_4$ shows a more rounded profile, obscuring the redox reactions. In addition, the specific capacity and stability values obtained (Fig. 4E and F) are more promising for the carbon-coated material. The pure $LiFePO_4$ flakes initially displayed a specific discharge capacity of 28 mAh g^{-1}, retaining only 41% of the initial capacity after 200 cycles. After the introduction of carbon through the carbon coating, the material's initial capacity increased to 124 mAh g^{-1} with a corresponding capacity retention of 73% after 200 cycles. Hence, subsequent experiments employed only carbon-coated $LiFePO_4$. The non-carbon-coated material appears unable to compensate for structural changes or deliver adequate

Table 1 The concentration of the various cations in the LFP leaching solution before and after pH adjustment *via* different detergents. '–' indicates values below the detection limit, and '/' indicates that this cation was not tested

		Al (mM)	Li (mM)	Fe (mM)	Ca (mM)	Na (mM)	K (mM)
LFP cathode leaching solution	Before pH adjustment	51.15 ± 0.85	35.27 ± 0.27	106.06 ± 2.11	0.0369 ± 0.0006	0.421 ± 0.002	/
	After pH adjustment with $Ca(OH)_2$	0.0296 ± 0.0020	32.98 ± 0.33	0.84 ± 0.04	1733.83 ± 22.25	/	/
LFP cathode leaching solution	Before pH adjustment	51.15 ± 0.85	35.27 ± 0.27	106.06 ± 2.11	0.0369 ± 0.0006	0.421 ± 0.002	/
	After pH adjustment with NH_4OH	–	28.56 ± 0.44	6.84 ± 0.10	–	0.420 ± 0.002	/
LFP cathode leaching solution	Before pH adjustment	51.15 ± 0.85	35.27 ± 0.27	106.06 ± 2.11	0.0369 ± 0.0006	0.421 ± 0.002	/
	After pH adjustment with NaOH	–	30.80 ± 0.16	–	0.0093 ± 0.0001	3853.58 ± 21.75	10.148
LFP cathode leaching solution	Before pH adjustment	51.15 ± 0.85	35.27 ± 0.27	106.06 ± 2.11	0.0369 ± 0.0006	0.421 ± 0.002	/
	After pH adjustment with KOH	0.008 ± 0.001	35.76 ± 0.29	0.586 ± 0.011	0.0316 ± 0.0014	20.220 ± 0.187	2805.749 ± 42.976

electronic conductivity during cycling. The addition of carbon, however, overcomes these limitations, ensuring efficient charge and mass transport within the material.[33]

3.3.2. Effect of competing ions on electrochemical performance. As a next step, we explored how adjusting the pH of the leaching solution using different bases impacts the electrochemical performance of $LiFePO_4$ electrodes. Fig. 5 shows the corresponding cyclic voltammograms and stability curves. The cyclic voltammograms, conducted within a voltage range of −0.3 V to +0.6 V *vs.* Ag/AgCl at a scan rate of 1 mV s^{-1}, demonstrate that all solutions support the electrochemical process of reversible ion intercalation into the $LiFePO_4$ host. However, there are noticeable differences in efficiency and stability.

We used $Ca(OH)_2$, an affordable and readily available base, to neutralize the leaching solution by adding a small amount of $Ca(OH)_2$ powder. After filtering out the precipitated components, we obtained a slightly yellowish-clear solution. The initial cyclic voltammogram (Fig. 5A) showed a strong oxidation response in the first cycle, followed by a small reduction peak that vanished subsequently. This indicates the release of naturally stored ions from the host structure. Subsequent cycles displayed typical patterns of lithium intercalation into the $LiFePO_4$ electrode, suggesting a highly reversible process. However, the expected capacity delivered was slightly lower than that of the cyclic voltammogram with the artificial electrolyte. Long-term cycling tests revealed an initial discharge capacity of 49 mAh g^{-1}, which quickly dropped to 25 mAh g^{-1} and remained stable for 500 cycles. The variations in values between the original and artificial leaching solutions are primarily due to trace components present in the original solution, absent in the artificial solution (such as organic residues and minute interfering ions). Furthermore, pH adjustments led to a higher concentration of competing ions compared to lithium ions, significantly complicating the process (35 mM Li^+ compared to 1734 mM Ca^{2+}).

To devise an effective method that minimally impacts the stability of the $LiFePO_4$ electrode while selectively uptaking pure lithium, we explored the influence of various added ions on the electrochemical performance. This evaluation aimed to assess the impact of different cations by employing a range of diverse ions, testing their monovalent, divalent, and trivalent properties, as well as their varied ionic radii. Initially, we employed $Al(OH)_3$, which is a trivalent ion with an ionic radius of 68 pm (compared to 90 pm for lithium). Since $Al(OH)_3$ is a weak base, the amount of added salt was quite high. The shape of the obtained cyclic voltammogram (Fig. 5B) appeared angular, featuring more pronounced spikes compared to the typical redox reactions observed in $LiFePO_4$.

Furthermore, both redox peaks were shifted towards higher potentials, suggesting a slower reaction/kinetics or a shifted potential. This observation was reinforced by examining the charge and discharge curves (Fig. S2), indicating difficulties in reaching the lower potential limit of −0.3 V *vs.* Ag/AgCl while the charging cycles proceeded normally. This discrepancy led to unfavorable outcomes, including low stability and specific capacity.

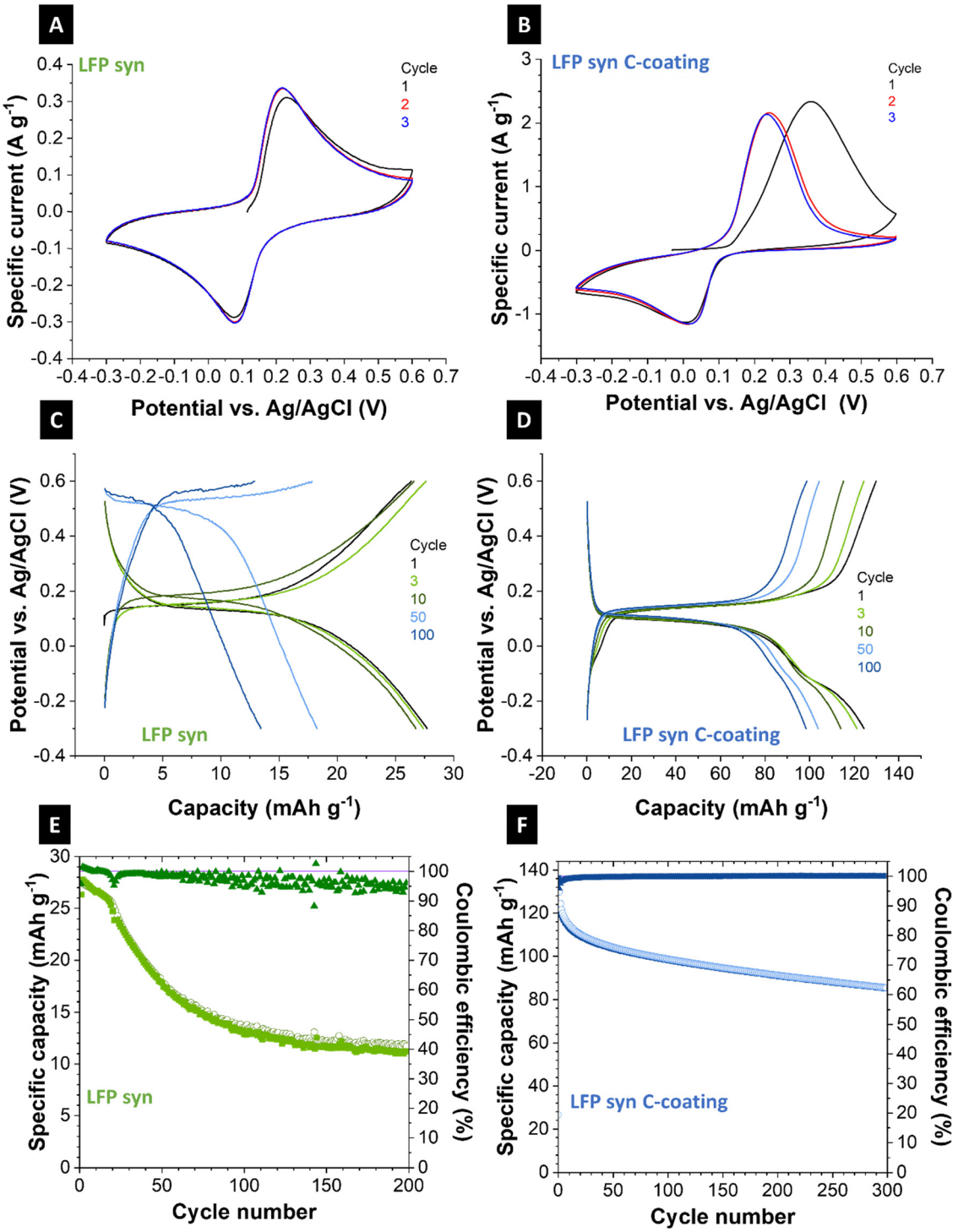

Fig. 4 Electrochemical performance of the $LiFePO_4$ electrode with and without carbon coating. 1st, 2nd, and 3rd cycles of the cyclic voltammograms at a scan rate of 1 mV s^{-1} in a potential range from −0.3 V to +0.6 V *vs.* Ag/AgCl for (A) as-synthesized $LiFePO_4$ electrode and (B) carbon-coated $LiFePO_4$. Charge and discharge profiles of the different cycles of $LiFePO_4$ at a specific current of 0.05 A g^{-1} for (C) as-synthesized $LiFePO_4$ electrode and (D) carbon-coated $LiFePO_4$. Cycling stability at a specific current of 0.05 A g^{-1} for (E) as-synthesized $LiFePO_4$ electrode and (F) carbon-coated $LiFePO_4$.

To address this, a non-metal salt (NH_4OH) was introduced for pH adjustment in the subsequent step. The initial electrochemical characterization *via* cyclic voltammogram (Fig. 5C) yielded symmetric and reversible curves, indicating a more promising outcome. However, even at this stage, significant performance collapses were observed during the stability tests.

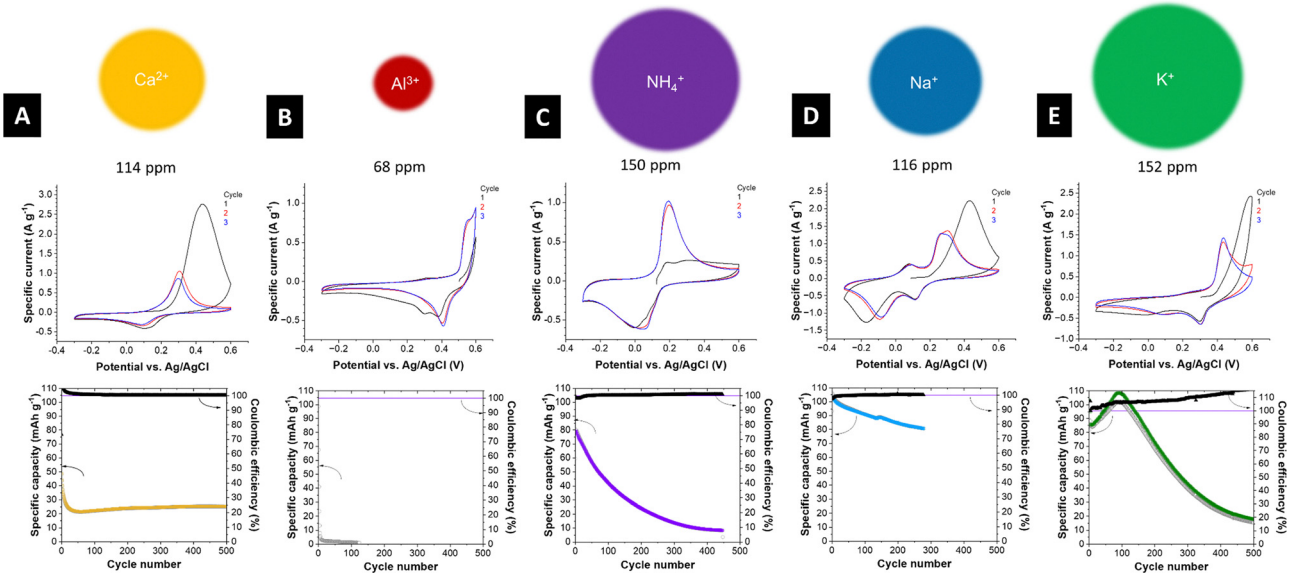

Fig. 5 Electrochemical performance of the $LiFePO_4$ electrode with carbon coating in different electrolytes showing 1st, 2nd and 3rd cycles of the cyclic voltammograms at a scan rate of 1 mV s^{-1} in a potential range from −0.3 V to +0.6 V *vs.* Ag/AgCl and corresponding cycling stability conducted at 50 mA g^{-1} for (A) $Ca(OH)_2$ adjusted $LiFePO_4$ battery leaching solution, (B) $Al(OH)_3$-adjusted $LiFePO_4$ battery leaching solution, (C) NH_4OH adjusted $LiFePO_4$ battery leaching solution, (D) NaOH-adjusted $LiFePO_4$ battery leaching solution, and (E) KOH-adjusted $LiFePO_4$ battery leaching solution.

While the initial capacity was around 80 mAh g^{-1}, subsequent cycles exhibited notable instability, resulting in a capacity of 42 mAh g^{-1} (53% capacity retention) after 100 cycles and 24 mAh g^{-1} (30% capacity retention) after 200 cycles.

Sodium ions, which share a very similar intercalation chemistry to lithium, exhibited symmetric cyclic voltammogram (Fig. 5D) patterns, displaying an initial higher release of lithium from the $LiFePO_4$ structure. The distinctive aspect of this cyclic voltammogram pattern is its depiction of not only the lithium intercalation but also a secondary intercalation feature at +0.08 V *vs.* Ag/AgCl and −0.09 V *vs.* Ag/AgCl, attributable to sodium ion intercalation into the $LiFePO_4$ host. This suggests a non-selective uptake when the sodium ion concentration exceeds that of lithium, highlighting a specific scenario. Regarding cycling stability, an initial discharge capacity of 106 mAh g^{-1} was recorded, followed by 91 mAh g^{-1} (86% capacity retention) after 100 cycles and 85 mAh g^{-1} (80% capacity retention) after 200 cycles. While this solution exhibits the best stability observed thus far, it implies that further ions may be integrated, which could hinder selective uptake. Exploring larger alkali metal ions, such as potassium, within this study revealed distinct cyclic voltammogram curves (Fig. 5E), indicating interactions with lithium.

Additionally, a barely pronounced characteristic plateau emerged, suggesting potassium intercalation into the $LiFePO_4$ structure. This interaction is much less pronounced since potassium ions have a much larger ionic radius, and the intercalation is not preferred, even in much higher concentrations compared to lithium ions. The galvanostatic charge and discharge data consistently show a greater release of lithium ions than their uptake. This distinct behavior is illustrated in the long-term cycling graph, which shows an initial increase in capacity within the first 100 cycles. Initially, the capacity starts at 85 mAh g^{-1}, increasing to 109 mAh g^{-1} after 100 cycles, indicating a capacity increase of 128%. Subsequently, the capacity gradually declines, stabilizing at 69 mAh g^{-1} (81% of the initial capacity) by the 200th cycle. Although the Coulombic efficiency values for all samples are consistently at around 100%, this particular case starts at 100% and gradually increases during cycling, reaching 107% by the 200th cycle. This phenomenon signifies a continuous release of more ions from the host material than were uptaken before, or potential additional side reactions occurring throughout the cycling process.

3.4. Lithium-ion removal performance

The selectivity assessment of LFP was conducted using a flow-through electrochemical cell configuration, enabling continuous electrolyte circulation during operation. A photograph of the setup is shown in Fig. S1. The electrochemical behavior using cyclic voltammetry and galvanostatic charge/discharge measurements of the LFP electrode was evaluated in the original LFP leaching solutions electrolytes with pH adjustment *via* NaOH, KOH, NH_4OH, and $Ca(OH)_2$ (Fig. 6). Fig. 6A, D, G and J show the cyclic voltammograms recorded over three consecutive cycles at a fixed scan rate. The cyclic voltammograms reveal distinct redox behaviors for each pH adjustment, with variations in peak intensities and shapes suggesting differences in electrochemical kinetics, reversibility, and charge storage mechanisms. At the same time, all examples exhibit quasi-reversible redox peaks, indicating the presence of Faradaic charge storage mechanisms. For the electrolyte adjusted with

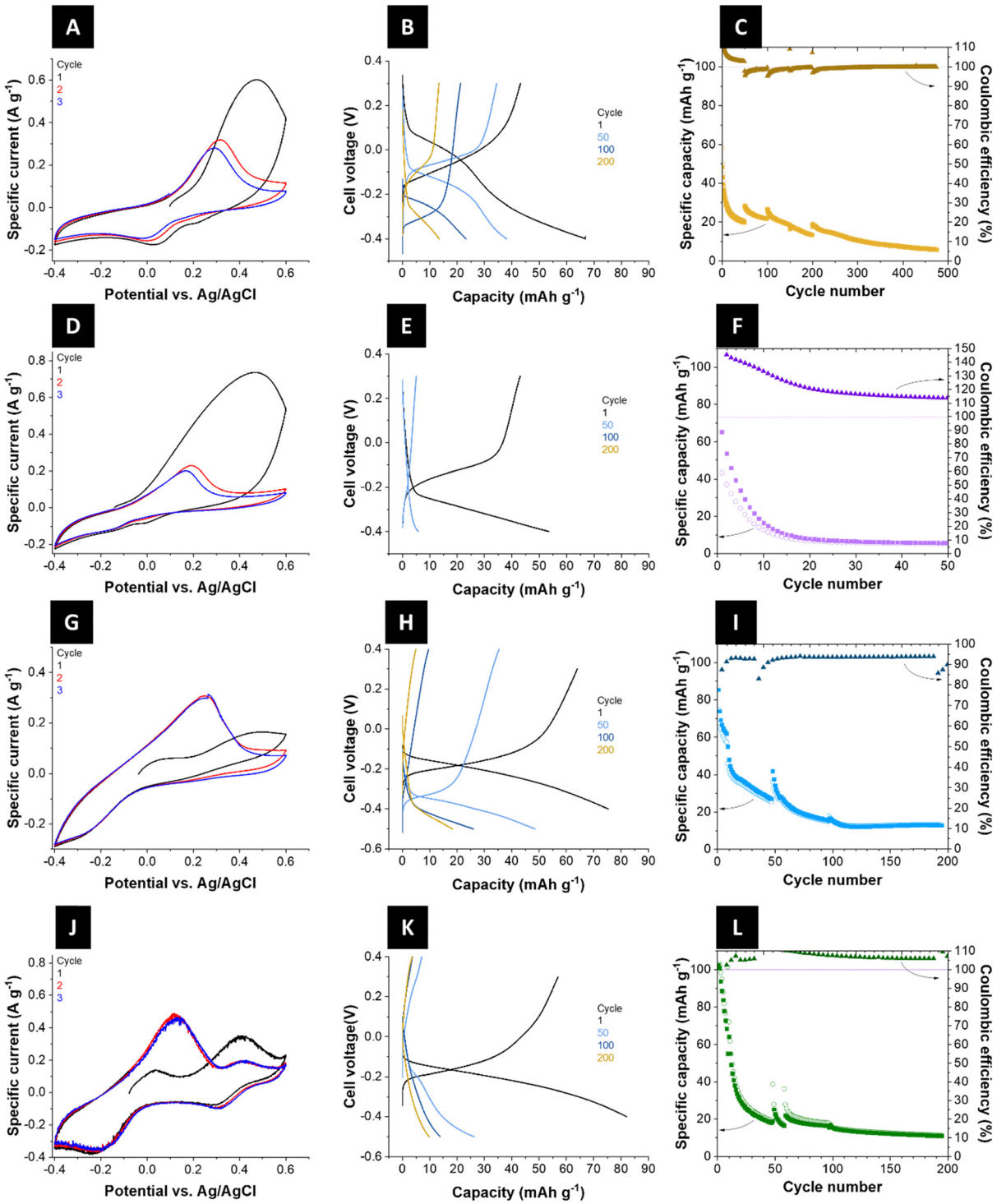

Fig. 6 Electrochemical performance of lithium recycling of the $LiFePO_4$ electrode in a spent LFP battery leaching solution. 1st, 2nd, and 3rd cycles of the cyclic voltammograms at a scan rate of 1 mV s^{-1} in a potential range from −0.4 V to +0.6 V *vs.* Ag/AgCl, including cycling stability conducted at 30 mA g^{-1} for (A)–(C) $Ca(OH)_2$ adjusted $LiFePO_4$ battery leaching solution, (D)–(F) $Al(OH)_3$ adjusted $LiFePO_4$ battery leaching solution, (G)–(I) NH_4OH adjusted $LiFePO_4$ battery leaching solution, (C) NaOH adjusted $LiFePO_4$ battery leaching solution, and (J)–(L) KOH adjusted $LiFePO_4$ battery leaching solution.

$Ca(OH)_2$ and NH_4OH, the current peak decreases slightly with cycling, suggesting initial activation followed by minor electrochemical stabilization. The broader peak separation in NH_4OH compared to $Ca(OH)_2$ implies differences in ion diffusion kinetics and charge transfer resistance. The cyclic voltammetry profile for the leaching solution with NaOH shows well-defined redox peaks, suggesting reversible electrochemical processes. The moderate peak currents indicate a balanced

electron and ion transfer kinetics. A slight shift in peak positions over consecutive cycles could reflect structural adjustments in the active species or gradual modifications in the electrode surface chemistry. This behavior suggests a relatively stable electrochemical environment.

In contrast, the cyclic voltammetry profile of the KOH-adjusted solution exhibits higher current responses and more pronounced redox peaks, indicating enhanced electrode reactivity. This could result from improved conductivity or a more favorable chemical environment for charge transfer. However, the increased specific current may also indicate side reactions, such as the intercalation of potassium ions alongside lithium ions. The high reversibility of the redox processes suggests that KOH creates an electrochemical environment that better facilitates charge storage and redox activity compared to NaOH.

The charge–discharge profiles of the LFP leaching solutions adjusted with $Ca(OH)_2$, NH_4OH, NaOH, and KOH reveal substantial differences in electrochemical behavior, indicating the influence of the different competing ions environment on charge storage mechanisms. For the $Ca(OH)_2$-adjusted electrolyte (Fig. 6B), the voltage profiles show significant polarization with steep voltage drops and irregular capacity retention over cycles, suggesting high internal resistance and possible passivation effects. The limited capacity retention and distorted charge–discharge curves imply poor electrochemical reversibility, likely due to the formation of insulating precipitates that hinder ion transport. The NH_4OH-adjusted system (Fig. 6E) exhibits a more stable voltage profile with lower polarization compared to $Ca(OH)_2$. However, the relatively low specific capacity and the progressive decline in voltage plateaus over cycles indicate moderate capacity degradation. The presence of ammonium ions may influence reaction equilibria and solubility, affecting ion mobility and charge storage efficiency.

In contrast, the NaOH-adjusted system (Fig. 6H) demonstrates improved electrochemical performance, characterized by more defined voltage plateaus and better capacity retention over multiple cycles. The reduced polarization suggests enhanced charge transfer kinetics, likely due to better solubility of active species and improved electrolyte–electrode interactions.[43–45] However, a gradual shift in voltage curves over extended cycling indicates minor structural transformations or side reactions.

The KOH-adjusted system (Fig. 6K) exhibits comparable characteristics to the NaOH-based system, with well-defined voltage plateaus, minimal polarization, and superior capacity retention in initial cycles. The strong alkaline nature of KOH and NaOH likely enhances ion conductivity and prevents excessive passivation, leading to improved cycling stability. The long-term cycling stability and Coulombic efficiency of the different pH-adjusted leaching solutions further illustrate their impact on electrochemical durability.

The $Ca(OH)_2$-adjusted electrolyte system (Fig. 6C) obtains an initial capacity of 50 mAh g^{-1} and displays severe capacity fading over cycling, with rapid performance deterioration and poor Coulombic efficiency. This suggests the formation of passivating surface layers or dissolution of active species, leading to irreversible capacity loss with a capacity retention of 50% after 100 cycles. The instability in Coulombic efficiency indicates the presence of continuous side reactions and poor charge retention.

The NH_4OH adjusted system (Fig. 6F) shows slightly improved cycling stability compared to $Ca(OH)_2$, with an initial capacity of 65 mAh g^{-1}, but suffers from more significant capacity fading, leading to a capacity retention of only 9% after 50 cycles. The first cycle has a high Coulombic efficiency (140%), meaning extra ions are released from the LFP structure. However, the efficiency drops over time, likely due to electrode wear or loss of active material. The NaOH-adjusted system (Fig. 6I) demonstrates better cycling performance, with a more gradual capacity fade and relatively stable coulombic efficiency at 94% over extended cycles. The initial capacity reaches 85 mAh g^{-1}, and the higher retention of specific capacity at 50 cycles, with 50% and 22% remaining after 100 cycles, suggests improved structural stability and mitigated side reactions. However, some degradation effects remain evident over prolonged cycling. The KOH-adjusted system (Fig. 6L) exhibits the most stable cycling behavior within our testing series, with an initial capacity of 102 mAh g^{-1} and capacity retention of 50% after 50 cycles and 15% after 100 cycles. The Coulombic efficiency values higher than 100% indicate the parasitic reactions.

The comparative analysis highlights the critical role of alkaline pH adjustment in determining the electrochemical performance of LFP leaching solutions. $Ca(OH)_2$ and NH_4OH lead to significant capacity fading and poor cycling stability, likely due to passivation effects, electrode degradation, or unfavorable reaction equilibria. To evaluate the long-term lithium-ion recovery performance of the LFP-based electrode, lithium removal capacities and selectivity factors were assessed over 200 cycles in the LFP leaching solution pH adjusted with $Ca(OH)_2$, KOH, and NaOH (Table 2). For the $Ca(OH)_2$ adjusted system, the lithium removal capacity achieved values of 9.0 $mg_{Li}\ g_{LFP}{}^{-1}$, decreasing to a value of 6.1 $mg_{Li}\ g_{LFP}{}^{-1}$ after 100 cycles. At the same time, the carbon-coated $LiFePO_4$ uptake electrode takes up amounts of Ca^{2+} ions (29.9 $mg_{Ca}\ g_{LFP}{}^{-1}$). However, if the increased initial concentration is considered, the lithium-to-calcium selectivity factor ($K_{Li/Ca}$) of 89.3 exhibited a preferred uptake of lithium before calcium. The value of the selectivity factor decreases during the cycling, suggesting a gradual loss of lithium selectivity, likely due to competitive adsorption effects or electrode degradation.

In contrast, NaOH and particularly KOH create more favorable electrochemical environments with improved charge transfer kinetics, enhanced reversibility, and superior long-term stability. This leads to an improved lithium removal capacity of 22.6 $mg_{Li}\ g_{LFP}{}^{-1}$ in the first cycle, 17.7 $mg_{Li}\ g_{LFP}{}^{-1}$ in the 10^{th} cycle, and 13.9 $mg_{Li}\ g_{LFP}{}^{-1}$ in the 50^{th} cycle. After 100 cycles, a drastic decline in lithium removal capacity was observed, reaching only 6.8 $\mu g_{Li}\ g_{LFP}{}^{-1}$. Sodium uptake increased significantly over time, reaching 1.9 $g_{Na}\ g_{LFP}{}^{-1}$ at 50 cycles, highlighting a strong preference shift toward Na^+ uptake. This trend is also reflected in the selectivity values,

Table 2 Selectivity factors, removal capacities, and discharge capacities of electrochemical recovery experiments in different pH-adjusted leaching solutions. '–' indicates values below the detection limit, and '/' indicates that this cation was not tested

Cycle	$K_{Li/Ca}$	Removal capacity ($mg_{Li}\ g_{LFP}^{-1}$)	Removal capacity ($mg_{Ca}\ g_{LFP}^{-1}$)	Discharge capacity (mAh g^{-1})
1	89.3	9.0	26.9	43
50	56.8	6.1	24.9	35
100	23.1	6.1	23.7	22
200	/	4.1	7.7	13

Cycle	$K_{Li/Na}$	Removal capacity ($mg_{Li}\ g_{LFP}^{-1}$)	Removal capacity ($mg_{Na}\ g_{LFP}^{-1}$)	Discharge capacity (mAh g^{-1})
50	0.7	5.6	0.4	0.04
100	–	5.6	–	5
200	<0.1 (0.015)	3.8	12.5	/

Cycle	$K_{Li/Na}$	Removal capacity ($mg_{Li}\ g_{LFP}^{-1}$)	Removal capacity ($mg_{Na}\ g_{LFP}^{-1}$)	Discharge capacity (mAh g^{-1})
1	13.2	22.6	603	64
10	7.7	17.7	955	52
50	3.0	13.9	1909	36
100	0.4	<0.1 (0.0068)	37	10
200	1.4	1.9	573	5

Cycle	$K_{Li/K}$	Removal capacity ($mg_{Li}\ g_{LFP}^{-1}$)	Removal capacity ($mg_{K}\ g_{LFP}^{-1}$)	Discharge capacity (mAh g^{-1})
1	12.0	13.1	482.6	57
10	4.5	12.7	1233.0	42
50	1.0	3.0	1264.7	7
100	1.0	2.2	949.4	4
200	1.1	1.4	523.1	4

which decrease from 13.2 in the first cycle to only 3.0 after 50 cycles, confirming poor long-term selectivity.

A similar trend was observed for the electrolyte pH adjusted with KOH, where lithium removal capacity dropped from 13.1 $mg_{Li}\ g_{LFP}^{-1}$ in the first cycle to 12.7 $mg_{Li}\ g_{LFP}^{-1}$ after 10 cycles and 3.0 $mg_{Li}\ g_{LFP}^{-1}$ after 50 cycles, while potassium removal remained high. These findings align with the electrochemical cycling performance, where discharge capacities decreased from 43 mAh g^{-1} to 13 mAh g^{-1} in the presence of Ca^{2+}, from 57 mAh g^{-1} to 4 mAh g^{-1} with K^+, and from 64 mAh g^{-1} to only 5 mAh g^{-1} with Na^+. The most severe capacity fade was observed in the KOH-based electrolyte, where the discharge capacity dropped from 57 mAh g^{-1} to 4 mAh g^{-1} after 200 cycles, further supporting the hypothesis that larger cations, particularly K^+, contribute to irreversible electrode degradation. For the KOH system, the selectivity factors are comparable to those of the NaOH system, with initial values of 12, which rapidly decrease to only 1 after 50 cycles. Overall, the material demonstrated the highest lithium selectivity in the presence of calcium, followed by sodium, with potassium presenting the greatest competitive interference.

These results suggest that while NaOH-adjusted conditions initially provide better lithium selectivity and electrochemical performance, extended cycling leads to a significant loss of lithium recovery efficiency due to increasing competition from Na^+ and structural changes in the LFP electrode. Additionally, the highly probable interaction of polyethylene terephthalate-based anion exchange membrane with the electrolyte could contribute to side reactions that negatively impact electrochemical performance. This effect may be more pronounced in systems with weaker alkaline conditions, where the stability of ionic species and surface interactions play a crucial role in overall efficiency. These findings suggest that NaOH-adjusted leaching solutions offer the most promising performance for applications requiring high efficiency and durability.

3.5. Post mortem analysis

The structural and morphological stability of the carbon-coated $LiFePO_4$ electrode before and after electrochemical cycling was evaluated using X-ray diffraction and scanning electron microscopy. The X-ray diffractogram (Fig. 7A) confirms that the pristine carbon-coated $LiFePO_4$ electrode maintains the characteristic reflections of orthorhombic $LiFePO_4$ (*Pnma*, PDF 81-1173) along with the presence of strong reflections from graphitic carbon (PDF 41-1487) from the current collector. After cycling, the overall phase integrity of $LiFePO_4$ remains intact, though slight peak broadening and intensity variations suggest minor structural changes or possible amorphization effects.

A picture of the electrode (Fig. 7B) reveals a uniform black coating and no parts separating from the electrode, indicating a stable coating. Microstructural analysis *via* SEM (Fig. 7C and D) highlights notable surface alterations upon cycling that can be linked to the shifted voltage profile. While the pristine electrode exhibits a relatively compact and homogeneous morphology, the cycled electrode shows the formation of cracks and particle detachment, likely induced by volume expansion/contraction during lithiation and delithiation. Such degradation phenomena could contribute to increased internal resistance and capacity fading over prolonged cycling.

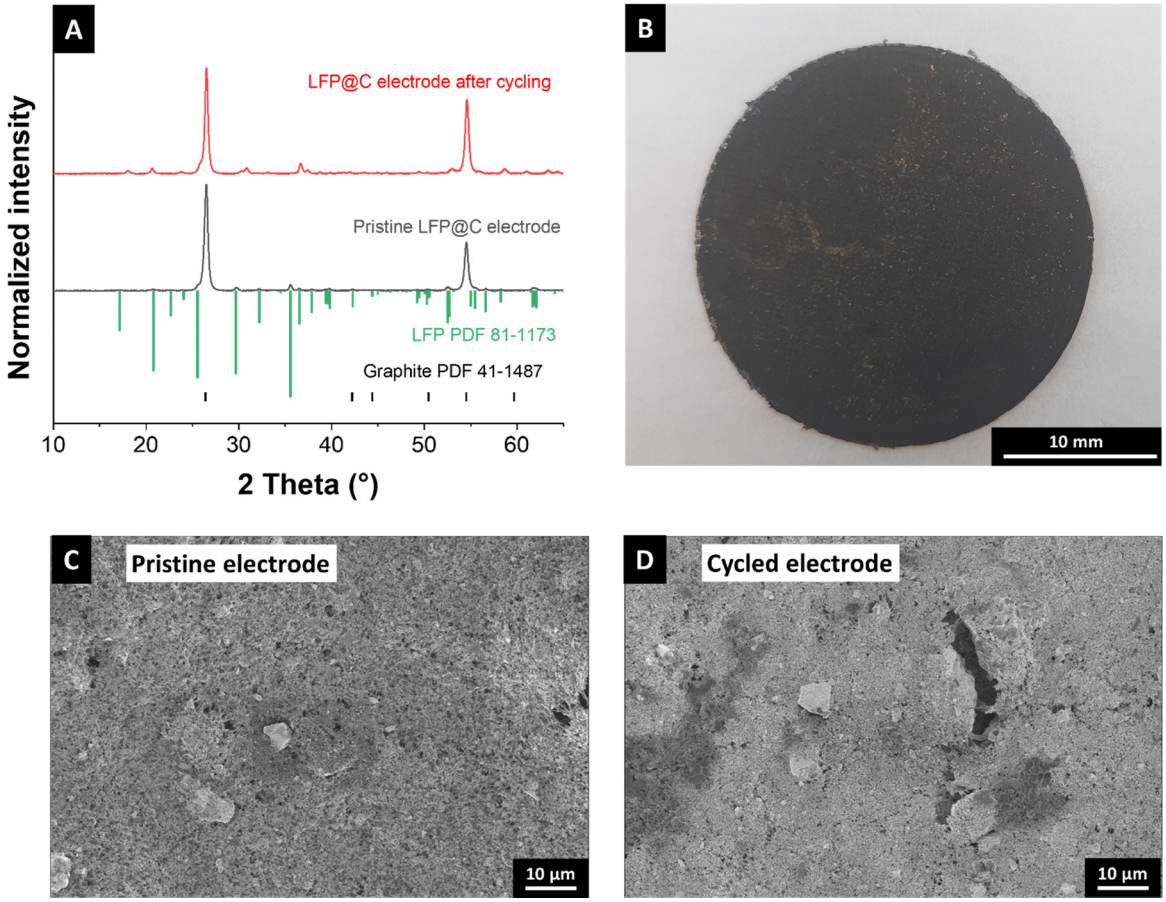

Fig. 7 Post mortem characterization after electrochemical lithium-ion recovery. (A) X-ray diffractograms using Cu-Kα radiation for the pristine electrode in comparison to the cycled electrode after 200 cycles. (B) Photograph of the cycled electrode. Scanning electron micrograph of (C) pristine $LiFePO_4$ and (D) cycled (200 cycles) $LiFePO_4$.

4. Conclusions

The growing demand for lithium-ion batteries in electric vehicles and portable electronics has intensified the need for sustainable and efficient recycling methods to recover critical materials, particularly lithium, from spent batteries. This study investigates the electrochemical recovery of lithium from spent lithium iron phosphate batteries using carbon-coated $LiFePO_4$ as a selective electrode material. $LiFePO_4$ nanoplates were synthesized *via* a solvothermal method and coated with carbon to enhance conductivity and stability. The material was characterized using X-ray diffraction, scanning electron microscopy, and Raman spectroscopy, confirming the formation of orthorhombic $LiFePO_4$ with a conductive carbon layer.

A leaching solution was prepared from spent LFP batteries through calcination and acid digestion, followed by pH adjustment using various bases ($Ca(OH)_2$, NH_4OH, KOH, NaOH, and $Al(OH)_3$). The electrochemical performance of carbon-coated $LiFePO_4$ was evaluated in both artificial and real leaching solutions. The results demonstrate that carbon-coated $LiFePO_4$ exhibits superior electrochemical performance, with an initial discharge capacity of 124 mAh g^{-1} and 73% capacity retention after 200 cycles. The pH of the leaching solution significantly influenced lithium-ion recovery efficiency, with NaOH-adjusted solutions showing the best performance, achieving an initial lithium removal capacity of 22.6 mg_{Li} $g_{LFP}{}^{-1}$. However, long-term cycling revealed a decline in lithium selectivity due to competing sodium-ion uptake. KOH-adjusted solutions exhibited higher initial capacities but suffered from severe capacity fading, attributed to the interference of potassium ions. Adjustments with $Ca(OH)_2$ and NH_4OH resulted in poor lithium selectivity and stability.

Post mortem analysis of cycled electrodes indicated minor structural changes and surface cracking, likely due to volume expansion during lithiation/delithiation. These findings underscore the importance of optimizing electrode materials and pH adjustment strategies to enhance electrochemical lithium-ion recovery efficiency and long-term stability. This work highlights the potential of electrochemical recycling as a sustainable and efficient method for recovering lithium from spent LFP batteries, contributing to the development of circular and environmentally friendly battery recycling systems.

Author contributions

Stefanie Arnold: conceptualization, methodology, investigation, data curation, visualization, writing – original draft,

and writing – review & editing. Volker Presser: conceptualization, supervision, validation, writing – review & editing, and funding acquisition.

Conflicts of interest

There are no conflicts to declare.

Data availability

Data are available *via* **https://doi.org/10.5281/zenodo.15731663**

Supporting Information contains additional electrochemical analysis.

Acknowledgements

We thank the INM Service Group Chemical Analytics (Andrea Jung) for the chemical analysis. VP acknowledges support for the eLiFlow project by the European Union from the European Regional Development Fund (EFRE) and the State of Saarland, Germany. VP and SA acknowledge funding from the EnFoSaar project (State of Saarland).

References

1 C. P. Grey and D. S. Hall, *Nat. Commun.*, 2020, **11**, 1–4.
2 Y. Ding, Z. P. Cano, A. Yu, J. Lu and Z. Chen, *Electrochem. Energy Rev.*, 2019, **2**, 1–28.
3 M. A. Hannan, M. M. Hoque, A. Hussain, Y. Yusof and P. J. Ker, *IEEE Access*, 2018, **6**, 19362–19378.
4 B. K. Sovacool, S. H. Ali, M. Bazilian, B. Radley, B. Nemery, J. Okatz and D. Mulvaney, *Science*, 2020, **367**, 30–33.
5 M. L. Vera, W. R. Torres, C. I. Galli, A. Chagnes and V. Flexer, *Nat. Rev. Earth Environ.*, 2023, **4**, 149–165.
6 E. Comission, Green Deal: EU agrees new law on more sustainable and circular batteries to support EU's energy transition and competitive industry, **https://ec.europa.eu/commission/presscorner/detail/en/ip_22_7588**, (accessed 02.01.2023).
7 B. E. Murdock, K. E. Toghill and N. Tapia-Ruiz, *Adv. Energy Mater.*, 2021, **11**, 2102028.
8 R. E. Ciez and J. F. Whitacre, *Nat. Sustainability*, 2019, **2**, 148–156.
9 J. Heelan, E. Gratz, Z. Zheng, Q. Wang, M. Chen, D. Apelian and Y. Wang, *JOM*, 2016, **68**, 2632–2638.
10 N. Nitta, F. Wu, J. T. Lee and G. Yushin, *Mater. Today*, 2015, **18**, 252–264.
11 P. H. Camargos, P. H. J. dos Santos, I. R. dos Santos, G. S. Ribeiro and R. E. Caetano, *Int. J. Energy Res.*, 2022, **46**, 19258–19268.
12 L. Kavanagh, J. Keohane, G. Garcia Cabellos, A. Lloyd and J. Cleary, *Resources*, 2018, **7**, 57.
13 B. Makuza, Q. Tian, X. Guo, K. Chattopadhyay and D. Yu, *J. Power Sources*, 2021, **491**, 229622.
14 B. Huang, Z. Pan, X. Su and L. An, *J. Power Sources*, 2018, **399**, 274–286.
15 B. Friedrich and L. Peters, Status and trends of industrialized Li-ion battery recycling processes with qualitative comparison of economic and environmental impacts, *22nd International Congress for Battery Recycling*, 2017, pp. 20–22.
16 J. C.-Y. Jung, P.-C. Sui and J. Zhang, *J. Energy Storage*, 2021, **35**, 102217.
17 A. Chagnes and B. Pospiech, *J. Chem. Technol. Biotechnol.*, 2013, **88**, 1191–1199.
18 Y. Yao, M. Zhu, Z. Zhao, B. Tong, Y. Fan and Z. Hua, *ACS Sustainable Chem. Eng.*, 2018, **6**, 13611–13627.
19 G. Harper, R. Sommerville, E. Kendrick, L. Driscoll, P. Slater, R. Stolkin, A. Walton, P. Christensen, O. Heidrich, S. Lambert, A. Abbott, K. Ryder, L. Gaines and P. Anderson, *Nature*, 2019, **575**, 75–86.
20 A. Boyden, V. K. Soo and M. Doolan, *Procedia CIRP*, 2016, **48**, 188–193.
21 P. Meshram, B. D. Pandey and T. R. Mankhand, *Waste Manage.*, 2015, **45**, 306–313.
22 Z. J. Baum, R. E. Bird, X. Yu and J. Ma, *ACS Energy Lett.*, 2022, **7**(2), 712–719.
23 S. Arnold, J. G. A. Ruthes, C. Kim and V. Presser, *EcoMat*, 2024, **6**, e12494.
24 C. Lupi, M. Pasquali and A. Dell'Era, *Waste Manage.*, 2005, **25**, 215–220.
25 N. M. Asl, S. S. Cheah, J. Salim and Y. Kim, *RSC Adv.*, 2012, **2**, 6094–6100.
26 J. S. Ribeiro, M. B. J. G. Freitas and J. C. C. Freitas, *J. Environ. Chem. Eng.*, 2021, **9**, 104689.
27 X.-J. Nie, X.-T. Xi, Y. Yang, Q.-L. Ning, J.-Z. Guo, M.-Y. Wang, Z.-Y. Gu and X.-L. Wu, *Electrochim. Acta*, 2019, **320**, 134626.
28 Y. Li, S. Arnold, S. Husmann and V. Presser, *J. Energy Storage*, 2023, **60**, 106625.
29 M. Pasta, A. Battistel and F. La Mantia, *Energy Environ. Sci.*, 2012, **5**, 9487–9491.
30 D.-H. Nam, B. M. Foster and K.-S. Choi, *ACS Energy Lett.*, 2025, **10**, 2934–2941.
31 Z. Li, Z. Peng, H. Zhang, T. Hu, M. Hu, K. Zhu and X. Wang, *Nano Lett.*, 2016, **16**, 795–799.
32 L. Wang, K. Frisella, P. Srimuk, O. Janka, G. Kickelbick and V. Presser, *Sustainable Energy Fuels*, 2021, **5**, 3124–3133.
33 Z. Ma, Y. Fan, G. Shao, G. Wang, J. Song and T. Liu, *ACS Appl. Mater. Interfaces*, 2015, **7**, 2937–2943.
34 D. Weingarth, M. Zeiger, N. Jäckel, M. Aslan, G. Feng and V. Presser, *Adv. Energy Mater.*, 2014, **4**, 1400316.
35 J. Yu, X. Wang, M. Zhou and Q. Wang, *Energy Environ. Sci.*, 2019, **12**, 2672–2677.
36 J. Hassoun, F. Bonaccorso, M. Agostini, M. Angelucci, M. G. Betti, R. Cingolani, M. Gemmi, C. Mariani, S. Panero and V. Pellegrini, *Nano Lett.*, 2014, **14**, 4901–4906.
37 M. Wang, K. Liu, S. Dutta, D. S. Alessi, J. Rinklebe, Y. S. Ok and D. C. W. Tsang, *Renewable Sustainable Energy Rev.*, 2022, **163**, 112515.

38 T. Satyavani, A. S. Kumar and P. S. V. S. Rao, *Eng. Sci. Technol., Int. J.*, 2016, **19**, 178–188.
39 W. Zhu, D. Liu, A. Paolella, C. Gagnon, V. Gariépy, A. Vijh and K. Zaghib, *Front. Energy Res.*, 2018, **6**, 66.
40 S. Arnold, L. Wang, R. Mertens, S. Wieczorek and V. Presser, *Sep. Purif. Technol.*, 2025, **367**, 132770.
41 R.-C. Wang, Y.-C. Lin and S.-H. Wu, *Hydrometallurgy*, 2009, **99**, 194–201.
42 L. Li, J. Lu, Y. Ren, X. X. Zhang, R. J. Chen, F. Wu and K. Amine, *J. Power Sources*, 2012, **218**, 21–27.
43 A. J. Bard, L. R. Faulkner and H. S. White, *Electrochemical methods: fundamentals and applications*, John Wiley & Sons, 2022.
44 M. Pasta, C. D. Wessells, Y. Cui and F. La Mantia, *Nano Lett.*, 2012, **12**, 839–843.
45 J. B. Goodenough and Y. Kim, *Chem. Mater.*, 2010, **22**, 587–603.